

# Pressure-driven gapped-to-gapless phase transition in a quantum antiferromagnet with large planar anisotropy

K. Yu. Povarov,<sup>1,\*</sup> D. E. Graf,<sup>2</sup> V. O. Garlea,<sup>3</sup> T. Sakurai,<sup>4</sup> S. Kimura,<sup>5</sup> H. Nojiri,<sup>5</sup>  
A. Paduan-Filho,<sup>6</sup> A. Zheludev,<sup>7</sup> J. Wosnitzer,<sup>1,8</sup> H. Ohta,<sup>9,10</sup> and S. A. Zvyagin<sup>1,†</sup>

<sup>1</sup>*Dresden High Magnetic Field Laboratory (HLD-EMFL) and Würzburg-Dresden Cluster of Excellence ct.qmat, Helmholtz-Zentrum Dresden-Rossendorf, 01328 Dresden, Germany*

<sup>2</sup>*National High Magnetic Field Laboratory, Tallahassee, Florida 32310, USA*

<sup>3</sup>*Neutron Scattering Division, Oak Ridge National Laboratory, Oak Ridge, TN 37831, USA*

<sup>4</sup>*Research Facility Center for Science and Technology, Kobe University, Kobe, 657-8501, Japan*

<sup>5</sup>*Institute for Materials Research, Tohoku University, Sendai 980-8578, Japan*

<sup>6</sup>*Instituto de Física, Universidade de São Paulo, 05315-970 São Paulo, Brazil*

<sup>7</sup>*Laboratory for Solid State Physics, ETH Zürich, Switzerland*

<sup>8</sup>*Institut für Festkörper- und Materialphysik, Technische Universität Dresden, 01062 Dresden, Germany*

<sup>9</sup>*Molecular Photoscience Research Center, Kobe University, Kobe 657-8501, Japan*

<sup>10</sup>*Graduate School of Science, Kobe University, Kobe 657-8501, Japan*

(Dated: June 28, 2023)

Strongly correlated electron systems can be driven to quantum critical points via various routes. Contrary to field-induced transitions of a gapped quantum antiferromagnet into the gapless ordered state (characterized by the  $z = 2$  dynamic critical exponent and a quadratic excitation dispersion), pressure-induced instabilities possess  $z = 1$  and a linear excitation spectrum, belonging to another universality class. Employing radio-frequency susceptibility technique, we demonstrate that in the tetragonal easy-plane quantum paramagnet  $\text{NiCl}_2 \cdot 4\text{SC}(\text{NH}_2)_2$  (aka DTN) the spin gap vanishes at about 4.3 kbar, suggesting the onset of antiferromagnetic order induced by pressure. Powder neutron diffraction measurements confirm that no lattice distortion occurs at this pressure and that the high spin symmetry is preserved. We are able to quantitatively describe the pressure-driven evolution of the critical fields and spin Hamiltonian parameters in DTN. The studies are complemented by high-pressure electron spin resonance measurements confirming the proposed scenario.

The subject of quantum phase transitions induced by parameters such as magnetic field, hydrostatic pressure, or even chemical substitution, is of central interest modern condensed-matter physics [1–4]. Quantum critical points (QCP), while strictly speaking reside at zero temperature, are typically affecting major parts of the corresponding phase diagrams. Magnetic insulators with their short-ranged interactions and well-controlled effective Hamiltonians offer an ideal playground for studying quantum criticality and associated unusual behavior of magnetic correlations [5–9].

Nowadays, great attention is attracted by antiferromagnetic order, induced by magnetic field in gapped quantum paramagnets. This quantum phase transition, known as “magnetic Bose–Einstein condensation (BEC)” [10–12], requires undistorted axial  $O(2)$  spin symmetry, which is impossible to achieve in a real crystal. However, in the tetragonal material  $\text{NiCl}_2 \cdot 4\text{SC}(\text{NH}_2)_2$  (DTN) the spin space symmetry is the closest possible approximation to a genuine  $O(2)$  symmetry, making it celebrated as a perfect candidate compound for magnetic BEC [13, 14]. Especially tantalizing is the possibility of achieving the spontaneous breaking of  $O(2)$  spin symmetry (i.e., the onset of magnetic order) without the aid of

magnetic field in DTN, keeping the spectrum degenerate [15]. Such transitions are known to exist in certain quantum magnets, and they belong to a different universality class than the field-induced ones [16–18]. The key distinction is the dynamic critical exponent being  $z = 2$  (quadratic spectrum) in the field-induced, and  $z = 1$  (linear spectrum) in the pressure-induced case [15, 17]. These two possibilities are illustrated in Fig. 1a. The “linear”  $z = 1$  QCP is very remarkable: it should have mean-field critical exponents [17], universal scaling of dynamic fluctuations [9], and, importantly, is a natural habitat for a well-defined order-parameter amplitude mode (also referred to as “Higgs” mode in condensed matter) [19].

A good realization of the  $z = 1$  QCP is actually hard to find. Most of the materials known to show such a transition ( $\text{TiCuCl}_3$  [16, 20, 21],  $\text{KCuCl}_3$  [22, 23],  $(\text{C}_4\text{H}_{12}\text{N}_2)\text{Cu}_2\text{Cl}_6$  [24–26], and  $(\text{C}_9\text{H}_{18}\text{N}_2)\text{CuBr}_4$  [27, 28]) suffer from unwanted anisotropies, that eventually lead to the Ising universality class criticality [29]. This does not seem to be the case for  $\text{CsFeCl}_3$  [30, 31], but there one has to deal with the geometric exchange frustration. All that makes the unfrustrated and simple case of DTN especially appealing. Previously, successful attempts of closing the spin gap in DTN with the help of chemical substitution were made [32, 33]. In this case, the parameters of the spin Hamiltonian experience local modifications [34–37]. Alas, according to the Harris criterion [38], the phase transition

\* k.povarov@hzdr.de; Previous address: Laboratory for Solid State Physics, ETH Zürich, Switzerland

† s.zvyagin@hzdr.de

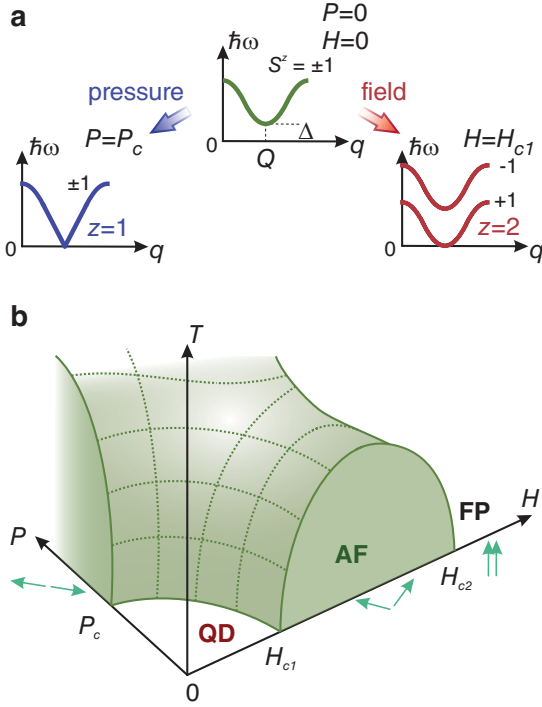


FIG. 1. (a) Evolution of excitation spectrum in a generic large- $D$  spin-1 quantum paramagnet, driven by hydrostatic pressure or longitudinal magnetic field. These two scenarios result in different types of critical point [15, 17]. The degenerate  $S^z = \pm 1$  doublet at zero field and pressure is shown in the middle; the spin gap  $\Delta$  is at  $\mathbf{Q} = (1/2, 1/2, 1/2)$  r.l.u. (b) Generic phase diagram of a gapped quantum paramagnet under the simultaneous action of field and pressure [16, 18], with the antiferromagnetically ordered phase (AF) shown as the green dome. Arrows show the spin arrangement in the corresponding phases; rotational symmetry is spontaneously broken in the AF state. Quantum-disordered (QD) and fully polarized (FP) states are gapped.

in  $\text{Ni}(\text{Cl}_{1-x}\text{Br}_x)_2 \cdot 4\text{SC}(\text{NH}_2)_2$  (DTNX) is sensitive to quenched disorder. This leads to a renormalization of the critical exponents, as was indeed observed experimentally [33, 39]. Thus, the quest for reaching an “ideal”  $z = 1$  quantum critical point in 3D is still open.

In the present study, we demonstrate a phase transition in DTN, that we ascribe to the long-sought  $z = 1$  QCP. This QCP resides at an accessible pressure of nearly 4.3 kbar. Neutron-diffraction measurements confirm the absence of a structural transition and reveal an undistorted tetragonal symmetry near this QCP (while there actually is an irreversible distortion of the lattice at higher pressures). We describe the experimentally measured phase boundaries employing linear spin-wave theory and quasi-1D numeric approximation, circumventing a renormalization of the DTN Hamiltonian parameters by quantum fluctuations. This allows us not only a qualitative understanding of the transition mechanism, but results in a complete quantitative picture.

The magnetic properties in DTN originate from the

spin-1  $\text{Ni}^{2+}$  ions, arranged on a body-centered tetragonal lattice (space group  $I4$ ) [40]. The complete crystallographic structure is displayed in Fig. 2a. The magnetic properties at low temperatures are defined by the competition between the strong single-ion planar anisotropy  $D$ , and the antiferromagnetic exchanges  $J_c$  and  $J_a$  along the corresponding directions. The effective Hamiltonian, graphically pictured in Fig. 2b, is:

$$\hat{\mathcal{H}} = \sum_{\mathbf{r}} D(\hat{S}_{\mathbf{r}}^z)^2 + J_c \hat{\mathbf{S}}_{\mathbf{r}} \hat{\mathbf{S}}_{\mathbf{r}+\mathbf{c}} + J_a (\hat{\mathbf{S}}_{\mathbf{r}} \hat{\mathbf{S}}_{\mathbf{r}+\mathbf{a}_1} + \hat{\mathbf{S}}_{\mathbf{r}} \hat{\mathbf{S}}_{\mathbf{r}+\mathbf{a}_2}). \quad (1)$$

Here,  $\mathbf{r}$  runs along the nickel positions in the tetragonal sublattice,  $\mathbf{a}$  and  $\mathbf{c}$  are the primitive translation vectors towards the nearest neighbors. Possible interactions between the two interpenetrating tetragonal sublattices are known to be frustrated and negligible [41]. Importantly, the symmetry prohibits any in-plane second-order anisotropic terms. The planar anisotropy protects the spin-singlet state  $|S^z = 0\rangle$  on every magnetic ion, thus preventing the Néel ordering, otherwise favored by the exchange interactions. This quantum-disordered state is labeled QD in Fig. 1b. The set of constants describing DTN at ambient pressure was initially obtained from zero-field neutron spectroscopy and thermodynamic studies [13, 42, 43], and later refined as  $D/k_B = 8.9$  K,  $J_c/k_B = 1.82$  K, and  $J_a/k_B = 0.34$  K [44] based on the spectroscopic properties at high magnetic fields (where the effect of quantum renormalization is not present). The zero-field gap  $\Delta/k_B \simeq 3.5$  K is relatively small compared to the overall  $S^z = \pm 1$  bosonic crystal-field excitations doublet bandwidth of nearly 8 K. If the magnetic field is applied along the  $c$  ( $z$ ) direction, the degeneracy of the doublet is removed due to Zeeman splitting. This is the well-understood mechanism of the “magnetic BEC” transition in DTN: closing the gap triggers the simultaneous onset of the low-temperature magnetic order at  $\mu_0 H_{c1} \simeq 2.1$  T [13, 45]. At stronger magnetic field  $\mu_0 H_{c2} \simeq 12.2$  T, a second transition occurs, corresponding to the full polarization (FP) of the spins. We would like to stress, that in DTN the zero-field gap is the consequence of single-ion anisotropy, in contrast to Heisenberg-like Haldane chain materials [46–48]. Thus, it happens to be a rare example of large- $D$  system (which can be distinguished, for instance, by the presence of characteristic single-ion magnon bound states in the FP phase [44, 47]).

As the pressure increases, the parameters of Hamiltonian (1) are expected to change. However, it is necessary to check first, whether the lattice remains undistorted and the general spin Hamiltonian structure is preserved. To this end, we have performed a series of structural neutron diffraction studies. As shown in Fig. 2c, the DTN lattice is smoothly compressed up to about 6 kbar at any temperature. Interestingly, despite the hydrostatic character of the pressure applied, the compression goes in a rather uniaxial manner, with mostly the lattice  $c$  constant shrinking ( $\partial c/\partial P = -0.038 \pm 0.003$  Å/kbar at 1.8 K). This implies the compression of the main Ni-

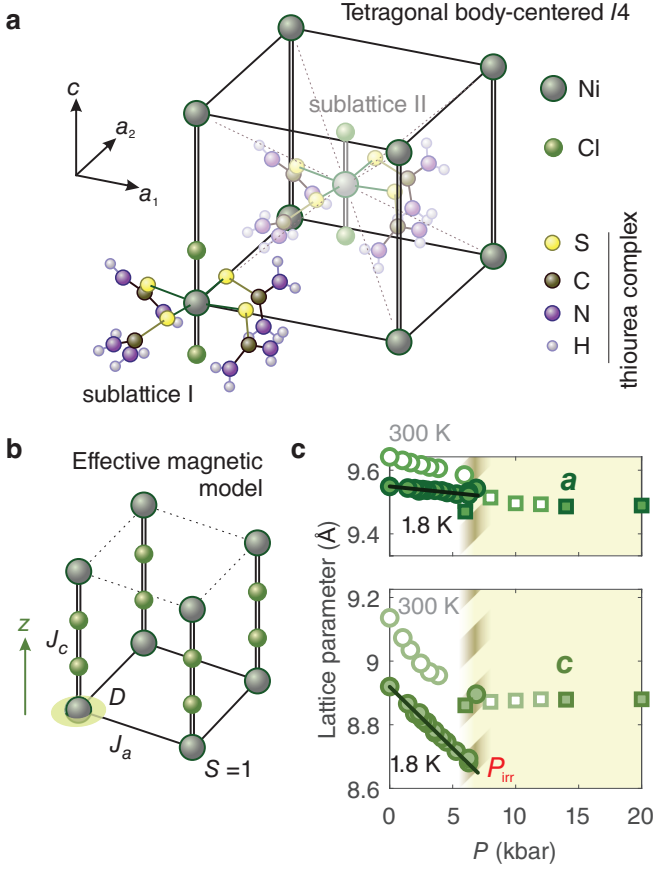


FIG. 2. (a) Crystal structure of DTN, with two  $\text{NiCl}_2 \cdot 4\text{SC}(\text{NH}_2)_2$  units per body-centered tetragonal cell. Only the nickel sites in the other corners belonging to sublattice I are shown for clarity. (b) Sketch of the relevant magnetic interactions in DTN. Only one of the two tetragonal sublattices are shown. (c) Change of the lattice parameters  $a$  and  $c$  with pressure, as measured by neutron diffraction. Open symbols correspond to room temperature, closed symbols to 1.8 K data. Circles and squares stand for data obtained in a gas and clamp pressure cell, respectively. This data was originally presented in Ref. [49].

Cl-Cl-Ni superexchange pathway and deformation of the  $\text{Ni}^{2+}$  local environment. Such changes must affect  $D$  and  $J_c$  in the first place. The lattice parameter  $a$  stays nearly constant with  $\partial a / \partial P = (-4.1 \pm 1.5) \cdot 10^{-3} \text{ Å/kbar}$ .

At  $P_{irr} \simeq 6 \text{ kbar}$ , an irreversible structural transition takes place, as evidenced by discontinuities in the lattice parameters. While the basic tetragonal block of the lattice is preserved, a double-period superstructure emerges due to the deformation of the thiourea  $\text{SC}(\text{NH}_2)_2$  ligands (see Supplemental Material and Ref. [49] for a more detailed discussion of this transition). In this situation the Hamiltonian (1) is not applicable anymore. However, as we show below, the range of pressures corresponding to reversible lattice compression is the one that contains the targeted QCP.

We can access the low-temperature phase diagram under pressure with the help of tunnel diode oscillator

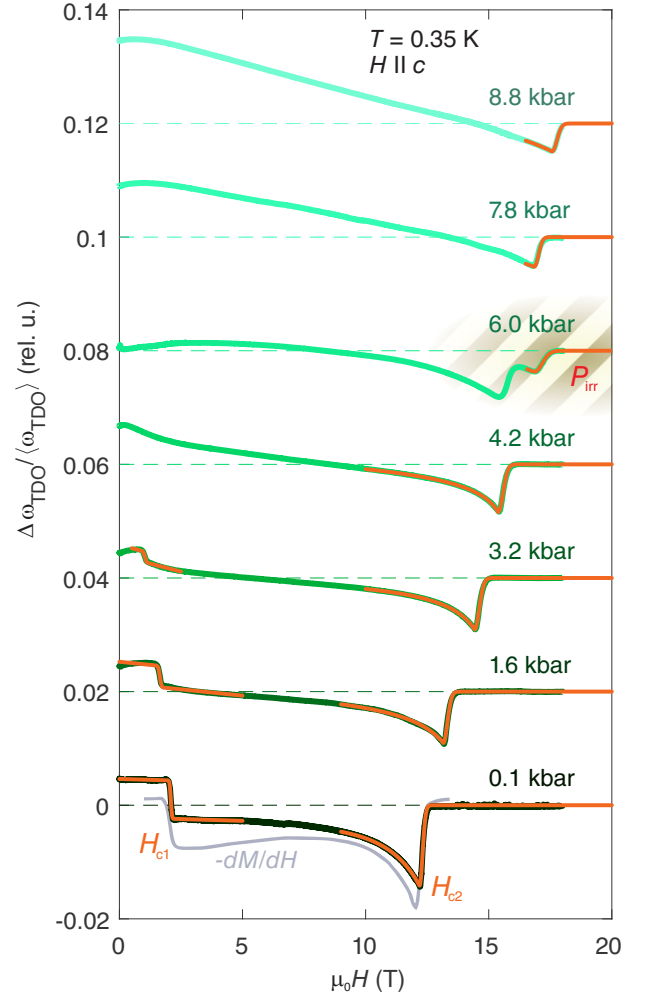


FIG. 3. Relative TDO frequency change at different pressures with background removed. An offset of 0.02 is introduced between the curves; the respective zero is shown as dashed line. Orange solid lines are fits (described in the Supplemental Material) to determine the exact position of the anomalies. The 0.1 kbar curve is downscaled by a factor of 2. In the background a reference  $dM/dH$  curve from Ref. [45] is shown.

(TDO) susceptibility measurements. This technique has already established itself as a versatile tool for detecting field-induced transitions in quantum magnets under applied pressure [50, 51]. While in general the observed relative frequency shift in a TDO circuit may have a contribution from both magnetic and dielectric permittivities, especially in a polar material such as DTN [52], the nearly-ambient-pressure data clearly resembles the well-known  $dM/dH$  dependence (see Fig. 3). The step-like and peak-like transitions at  $H_{c1}$  and  $H_{c2}$  are well discernible. With pressure applied, we observe a decrease and increase of the first and second critical fields, respectively. At 4.2 kbar, the  $H_{c1}$  transition is not visible anymore. The critical field  $H_{c2}$  increases linearly to  $P_{irr}$ , where a discontinuity appears. The curve at 6 kbar (about  $P_{irr}$ ) shows a split transition (Fig. 3) that re-

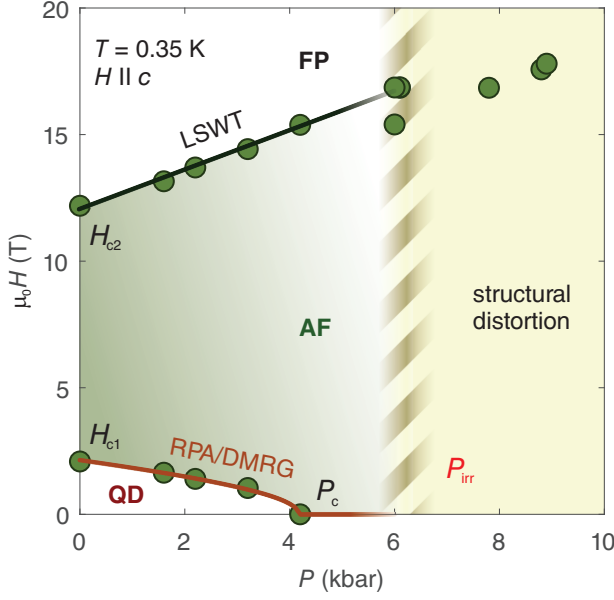


FIG. 4. Magnetic phase diagram of DTN. Points are obtained from TDO data, solid lines are the calculation results: Eq. (6) for the first critical field, and Eq. (2) for the second critical field. The region at which the structural distortion occurs is highlighted similar as in Fig. 2b.

flects the coexistence of two structurally different phases within the crystal. In the distorted phase, the saturation field continues to grow linearly with pressure, with nearly the same slope but shifted origin. The obtained pressure dependencies of  $H_{c1}$  and  $H_{c2}$  fields — the pressure-dependent phase diagram — is presented in Fig. 4.

The AF-FP phase boundary is known to follow the linear spin wave theory (LSWT) description without any quantum renormalization [44]:

$$g\mu_B\mu_0 H_{c2} = D + 4J_c + 8J_a. \quad (2)$$

Given the overall smallness of  $J_a$  and lack of a significant pressure-induced length change in this direction, we can neglect possible variations in this interaction. Thus, the phase-diagram evolution is due to the changes in  $D$  and  $J_c$  alone:

$$g\mu_B\mu_0 \frac{\partial H_{c2}}{\partial P} = \frac{\partial D}{\partial P} + 4\frac{\partial J_c}{\partial P}. \quad (3)$$

The spectroscopic measurements under applied pressure, that we discuss later, suggest that the  $g$  factor stays near its zero-pressure value 2.26. Thus, the measured slope  $\mu_0 \partial H_{c2} / \partial P = 0.78 \pm 0.03$  T/kbar (below the instability pressure) quantifies the linear dependence between the  $D$  and  $J_c$  parameters.

The analysis of the first critical field poses a much greater challenge: since  $g\mu_0\mu_B H_{c1} = \Delta$ , it requires evaluating the zero-field spin gap for the given set of Hamiltonian (1) parameters. No exact theory is available for

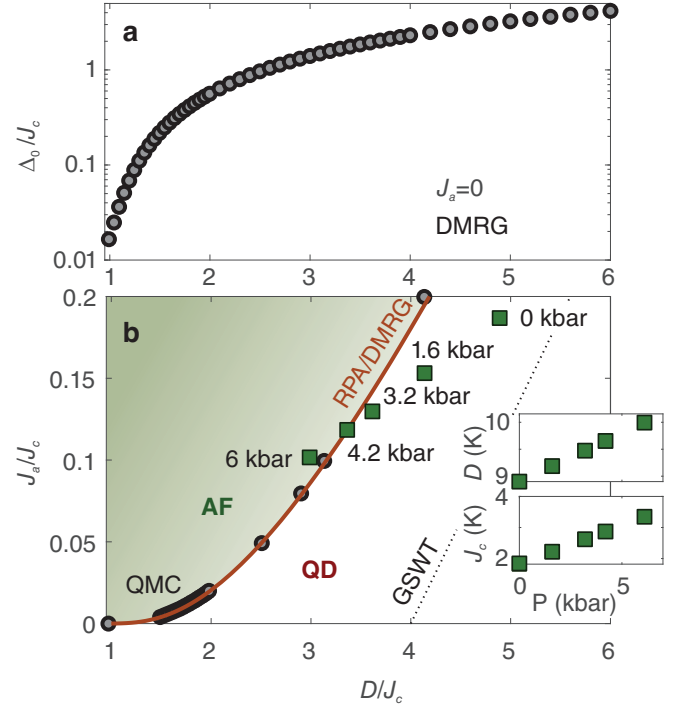


FIG. 5. (a) Spin-gap value vs anisotropy-to-exchange ratio in the single-chain limit, as obtained by DMRG calculations. (b) Phase diagram corresponding to the zero-field state of Hamiltonian (1). Black dots represent the QMC result [46]; the solid line is the prediction of our quasi-1D *ansatz*. The dotted line shows the 3D mean-field boundary between the QD and AF phases. Squares correspond to our estimate of the Hamiltonian (1) parameters at a given pressure. These are also independently shown in the inset.

that. We overcome this challenge employing a random-phase approximation (RPA) [53] based *ansatz* combined with density matrix renormalization group (DMRG) simulations [54–56]. The starting point is the determination of the zero-field gap value  $\Delta_0(D/J_c)$  in the  $J_a = 0$  limit of a single anisotropic chain, utilizing the latter technique. To the best of our knowledge, only a particular range close to the quantum critical point at  $D/J_c \sim 1$  was thoroughly accessed with DMRG earlier [57]. Our result is partially shown in Fig. 5(a). The next step of our *ansatz* is to apply the RPA treatment to interacting chains in order to estimate the critical value of the coupling  $J_a^{\text{crit}}$  that closes the gap. With details of the calculations (based on dynamic structure factor large- $D$  approximation [58, 59] and the Kramers–Kronig relations) given in the Supplemental Material, here we quote the key result:

$$J_a^{\text{crit}} = \frac{\Delta_0^2}{4AD}, \quad (4)$$

with  $1/4A \simeq 0.14$  provides an excellent description of the AF-QD phase boundary, previously obtained by extensive QMC simulations [46, 60], as can be seen in Fig. 5b.

This is a serious improvement compared to the common generalized spin-wave theory (GSWT) approximation [17] shown by the dotted line, that greatly underestimates the gap size near the critical line (and hence the predicted transition is significantly misplaced). Then, it follows from our *ansatz*, that the value of the gap, renormalized by  $J_a$ , is:

$$\Delta = \Delta_0 \sqrt{1 - \frac{J_a}{J_{\text{crit}}}}. \quad (5)$$

Hence, the first critical field can be expressed through the pressure-dependent Hamiltonian parameters as:

$$g\mu_0\mu_B H_{c1}(P) = \Delta \left( \Delta_0 \left( \frac{D(P)}{J_c(P)} \right), D(P) \right). \quad (6)$$

The ambient pressure  $H_{c1}$  is captured correctly by our *ansatz*, ensuring the validity of our approach for the smaller gap values as well.

The ability to correctly predict both critical fields using Eqs. (2) and (6) finally opens a route to a self-consistent treatment of the measured phase diagram without any “effective” parameters. We numerically optimize the agreement between our *ansatz* and the experimental  $H_{c1}$  data by varying the choice of the critical pressure  $P_c$  at which the gap closes completely. This fixes a unique combination of  $\partial(D, J_c)/\partial P$ . The optimization results in the critical pressure  $P_c = 4.3 \pm 0.3$  kbar (see Supplemental Material for more details). The magnetic phase diagram (Fig. 4) is fully captured with  $k_B^{-1}\partial D/\partial P = 0.16 \pm 0.03$  and  $k_B^{-1}\partial J_c/\partial P = 0.25 \pm 0.01$  K/kbar. Figure 5b illustrates how the parameters in the Hamiltonian (1) of DTN are pressure-tuned up to  $P_{\text{irr}}$ . The ground state is changing from QD to AF at  $P_c$  in accordance with the previous discussion.

Taking into account the experimentally known lattice compressibilities (see Supplemental Material [61]), we can directly obtain the magnetostriction coefficients. If  $z$  parameterizes the bond length in  $c$  direction, we find  $k_B^{-1}\partial D/\partial z = -4.1 \pm 0.7$  and  $k_B^{-1}\partial J_c/\partial z = -6.5 \pm 0.3$  K/Å. Surprisingly, they noticeably deviate from the set of magnetostriction coefficients (0 and  $-2.5$  K/Å) previously found at the ambient pressure by Zapf *et al* [42]. These latter values are clearly insufficient to describe the rapid growth of  $H_{c2}$  under pressure, yielding only 0.25 T/kbar — about 1/3 of the actual slope.

Not only the ground-state evolution under pressure is of interest, but the changes in spin dynamics as well. Electron spin resonance (ESR) has recently proved itself to be a valuable tool for quantum magnets spectroscopy under multiextreme conditions (low temperatures, high fields, applied pressure) [50, 62]. Selected examples of experimentally measured radiation transmission at various pressures are shown in Fig. 6a. The resonant modes (transmission minima), corresponding to single-magnon  $\Delta S^z = 1$  transitions with no momentum transfer remain

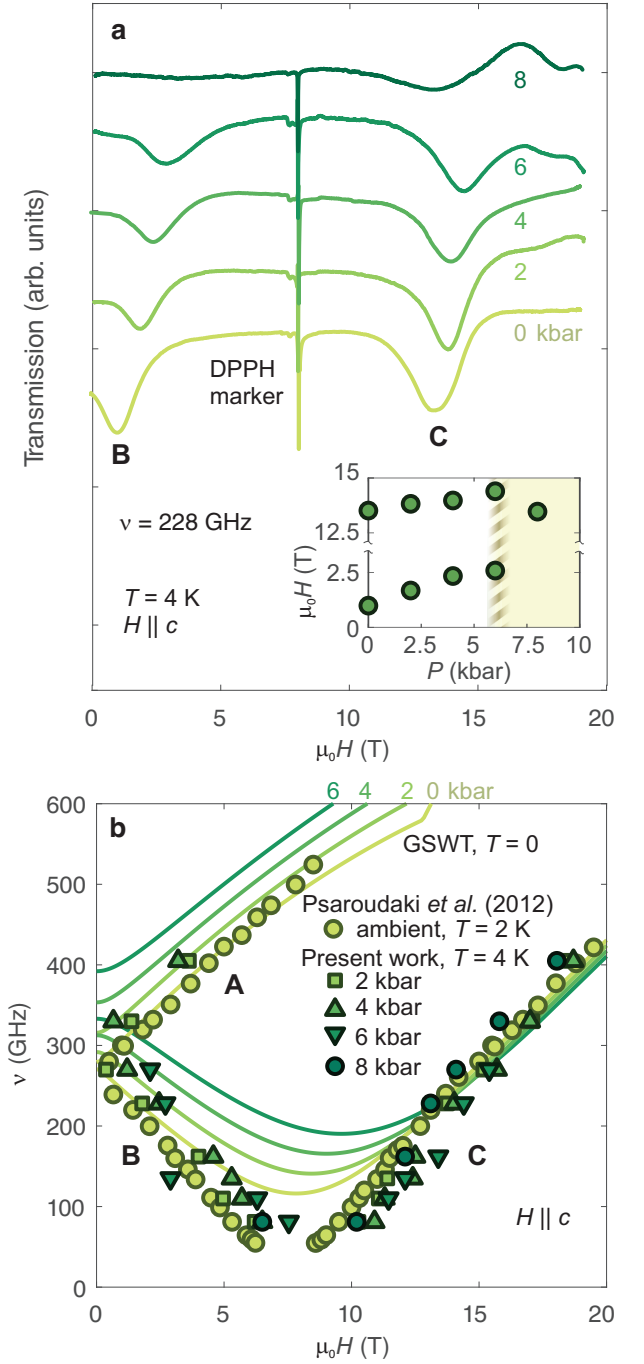


FIG. 6. (a) Main panel: Examples of  $T = 4$  K DTN ESR spectra at 228 GHz and various pressures. Transmission minima are spin resonances, the sharp line in the center is the DPPH (2,2-diphenyl-1-picrylhydrazyl), standard  $g = 2.00$  ESR marker. Inset: Pressure dependencies of modes B and C resonant fields at 228 GHz. (b) Frequency–field diagram of the DTN spin excitations under different pressures at 4 K. Ambient pressure data are taken from Ref. [44] (this set was measured near 2 K). Solid lines correspond to a  $T = 0$  GSWT description of the spin dynamics, using the estimated DTN parameters at the corresponding pressures.

well visible up to 6 kbar. With the pressure they experience a gradual shift towards higher fields, as illustrated in Fig. 6a inset. In the structurally distorted phase above about 6 kbar, the spectrum is affected more significantly.

The overall pressure-dependent ESR spectra of DTN inferred from such scans are present in Fig. 6b. We observe three branches (A, B, C), as indicated in the plot. The spectra change only qualitatively at pressures below  $P_{\text{irr}}$ . This is similar to small chemically-induced changes at  $q = 0$  Brillouin zone center of DTNX, seen by neutron [32, 33], and ESR [63] spectroscopy. The actual gap closing occurs at another, antiferromagnetic wavevector  $q = (1/2, 1/2, 1/2)$  r.l.u. To describe the spectra, we use the generalized spin-wave theory (GSWT) [15–17, 64]. It provides an interpolation between large- $D$  approach, suitable for QD state, and LSWT applicable in the high-field FP state (and possibly deep in the AF phase with  $1/S$  corrections included [65]). In contrast to these approaches, GSWT remains valid throughout the whole phase diagram in Fig. 1 (even though it predicts the misplaced QD-AF boundary due to the mean-field nature of this theory). The solid lines in Fig. 6b represent the predicted zero-temperature ESR single-magnon transitions for the Hamiltonian (1) parameters at different pressures. The temperature in the experiment was above the maximal  $T_N \simeq 1$  K (expected to occur in fields of about 8 T), and the description of the spectrum in the field range, corresponding to the low- $T$  AF phase is not accurate. At ambient pressure, the central part of the spectrum is known to show a strong temperature dependence between 2 and 0.5 K [41], eventually matching the theoretical prediction. In our case, the finite temperature precludes a quantitative comparison, but qualitatively the mildly changing spectra are consistent with the above analysis (e.g., pressure-induced shift to the right for the branch B, and to the left for the branch A in both theory and experiment). It would be highly desirable to explore the overall changes in the dynamics with the help of neutron spectroscopy. Alas, in the case of DTN this is a challenge due to the unfortunate scattering and field geometry required. Despite the great interest in the material, only a few such in-field studies are available even at ambient pressure [66–68].

The rich physics of DTN under pressure invites further investigations, related to the interplay of quantum and thermal fluctuations at  $z = 1$  quantum criticality [18, 21, 69, 70]. In particular, it would be important to access the order parameter (e.g., with neutron diffraction or nuclear magnetic resonance) and the complete field-temperature-pressure phase diagram. This would open the possibility to establish a direct connection between the minimalistic and highly symmetric spin Hamiltonian of DTN and the effective field theory used to describe the static and dynamic properties of critical quantum paramagnets [71–73]. The undistorted symmetry also makes DTN a perfect candidate investigating the effect of thermal and quantum fluctuations on the amplitude (“Higgs”) mode [21] in the absence of Ising-

type anisotropy. One can also expect chemically substituted DTNX to be a fruitful playground for the interplay of quantum  $z = 1$  criticality and quenched disorder, similarly to  $(\text{C}_4\text{H}_{12}\text{N}_2)\text{Cu}_2(\text{Cl}_{1-x}\text{Br}_x)_6$  [74–76],  $(\text{NH}_4)_x\text{K}_{1-x}\text{CuCl}_3$  [77], and  $\text{Cs}_{1-x}\text{Rb}_x\text{FeCl}_3$  [78]. The higher symmetry and a simpler, well-understood Hamiltonian make the case of DTNX much more appealing for such studies.

To summarize, we have identified the material DTN as a unique platform for studies of exotic  $z = 1$  universality physics. By means of several challenging measurement techniques we have confirmed the existence of pressure-induced critical point, separating gapped and gapless magnetic phases in the material. The nearly ideal axial symmetry of the structure is retained at that point, which makes DTN to stand out among the non-frustrated quantum paramagnets. In addition to that, we have extracted the pressure dependence of the spin Hamiltonian parameters from the data, and have achieved a quantitative theoretical understanding of the transition mechanism.

## METHODS AND TECHNIQUES

### $\text{NiCl}_2 \cdot 4\text{SC}(\text{NH}_2)_2$ samples

Samples for the thermodynamic measurements and the electron spin resonance spectroscopy were synthesized in the University of São Paulo from aqueous solution using thermal-gradient method [79].

Samples used in the neutron diffraction studies were synthesized at ETH Zürich. Fully deuterated chemicals (water and thiourea) were used [80]. The crystals were crushed into powder for these experiments.

### Neutron diffraction

The neutron diffraction experiments with the powder samples were performed at instrument HB2a at the High Flux Isotope Reactor, Oak Ridge National Laboratory (Tennessee, USA). Up to a few grams of deuterated DTN powder material were used. A Ge[113] or Ge[115] vertically focussing wafer-stack monochromator was used to produce a neutron beam with 2.41 Å or 1.54 Å wavelength, respectively. A  $^4\text{He}$  Orange cryostat with aluminum He-gas pressure cell (up to 6 kbar) and a CuBe clamp cell (6 to 20 kbar) was used. The pressure in the gas cell was measured *in situ* using a manometer. For the clamp cell a rock salt (halite) calibration curve was used for the pressure determination, resulting in an error bar of about 1 kbar. After initial data reduction, FULLPROF package [81] was used for the intensity profile analysis and structure determination. More details of these experiments can be found in Ref. [49].

## TDO susceptibility measurements

High-pressure radio-frequency measurements were conducted at the National High Magnetic Field Laboratory, Florida State University (Tallahassee, Florida, USA) in magnetic fields up to 18 T using a TDO susceptometer [82] tuned to operate at a resonant frequency near 2 MHz. The setup is similar to the one used in Ref. [50]. Magnetic field was applied along the  $c$  axis of the crystal placed in a tiny copper-wire coil with diameter 0.8 mm and height 1 mm. This assembly was immersed into Daphne 7575 oil (Idemitsu Kosan Co., Ltd.) and encapsulated in a Teflon cup inside the bore of a piston-cylinder chromium alloy (MP35N) pressure cell. The pressure created in the cell was calibrated at room temperature and again at low temperature using the fluorescence of the  $R1$  peak of a small ruby chip as a pressure marker [83] with accuracy better than 0.15 kbar. The pressure cell was immersed directly into  $^3\text{He}$ , allowing TDO measurements down to 350 mK.

## ESR measurements under pressure

High-pressure ESR studies of DTN were performed at the 25 T cryogen-free superconducting magnet ESR setup (25T-CSM) at the High Field Laboratory for Superconducting Materials, Institute for Material Research, Tohoku University (Sendai, Japan) [84, 85]. Gunn diodes were utilized as microwave sources up to 405 GHz; the transmitted radiation power was detected using a hot-electron InSb bolometer held at 4.2 K. DTN crystal was loaded into a Teflon cup filled with Daphne 7474 oil (Idemitsu Kosan Co., Ltd.) as pressure medium. A two-section piston-cylinder pressure cell made from NiCrAl (inner cylinder) and CuBe (outer sleeve) has been used. The inner pistons made of  $\text{ZrO}_2$  ceramics allow for low loss GHz radiation transmission. The applied pressure was calibrated against tin superconducting transition temperature [86], detected by AC susceptometer. The actual pressure during the experiment was calculated using the relation between the load at room temperature and the pressure obtained at around 3 K; the pressure calibration accuracy is better than 0.5 kbar [87].

## DMRG calculations

The DMRG calculations utilized the `Julia` version of the `ITensors` package [88, 89]. A 249-site anisotropic  $S = 1$  chain was simulated. The calculations were performed on the `hemera` cluster (HZDR).

## ACKNOWLEDGEMENTS

We thank A. Mannig, J. Möller, and G. Perren for their involvement at the early stage of the ETH Zürich

part of the project. This work was supported by the Deutsche Forschungsgemeinschaft, through ZV 6/2-2, the Würzburg-Dresden Cluster of Excellence on Complexity and Topology in Quantum Matter - *ct.qmat* (EXC 2147, project No. 390858490), SFB 1143 (project No. 247310070), as well as by HLD at HZDR, member of the European Magnetic Field Laboratory (EMFL). We also thank HZDR for providing access to the HPC cluster `hemera` where the calculations have been performed. The neutron diffraction experiments at HB2a used resources at the High Flux Isotope Reactor, a Department of Energy Office of Science User Facility operated by the Oak Ridge National Laboratory. This work was partially supported by the Swiss National Science Foundation, Division II. A portion of this work has been performed at the National Magnetic Field Laboratory, which is supported by the National Science Foundation Cooperative Agreement DMR-1644779 and the State of Florida. ESR experiments were performed at the High Field Laboratory for Superconducting Materials, Institute for Material Research, Tohoku University (proposal 19H0501 and 20H0501). Support of the ICC-IMR Visitor Program at Tohoku University is acknowledged. This work was partially supported by the Brazilian agencies CNPq (grant 304455-2021-0) and FAPESP (grant 2015-16191-5).

## COMPETING FINANCIAL INTERESTS

The authors declare no competing financial interests.

## DATA AVAILABILITY

The data that support the findings of this study are available from the corresponding author upon reasonable request.

## AUTHOR CONTRIBUTIONS

S.Z. conceived the project and performed the TDO (together with D.E.G.) and ESR (together with T.S., S.K., and H.N.) measurements; K.Yu.P. performed the analysis of this data and the numeric simulations. V.O.G. has performed the neutron diffraction measurements and analyzed the data. A.P.F. has synthesized the non-deuterated single crystals used in the study. H.O. and H.N., A.Z., and J.W. administered at the KU and TU, ETHZ, and HZDR parts of the project correspondingly. All the authors have contributed into the to the discussions and manuscript writing.

- 
- [1] S. Sachdev, *Quantum Phase Transitions* (Cambridge University Press, U.K., 2011).
- [2] M. Vojta, Quantum phase transitions, *Rep. Prog. Phys.* **66**, 2069 (2003).
- [3] S. Sachdev, Quantum criticality: Competing ground states in low dimensions, *Science* **288**, 475 (2000).
- [4] M. Continentino, *Quantum Scaling in Many-Body Systems*, 2nd ed. (Cambridge University Press, 2017).
- [5] B. Grenier and T. Ziman, Modern quantum magnetism by means of neutron scattering, *C. R. Physique* **8**, 717 (2007).
- [6] S. Sachdev, Quantum magnetism and criticality, *Nat. Physics* **4**, 173 (2008).
- [7] T. Giamarchi, Some Experimental Tests Of Tomonaga-Luttinger Liquids, *Int. J. Mod. Phys. B* **26**, 1244004 (2012).
- [8] D. A. Tennant, Studies of Spinons, Majoranas, and Monopoles in Spin Liquid and Quantum Critical Magnets with Neutrons, *J. Phys. Soc. Jpn.* **88**, 081009 (2019).
- [9] A. Zheludev, Quantum critical dynamics and scaling in one-dimensional antiferromagnets, *J. Exp. Theor. Phys.* **131**, 34 (2020).
- [10] E. G. Batyev and L. S. Braginskii, Antiferromagnet in a strong magnetic field: analogy with Bose gas, *Sov. Phys. JETP* **60**, 781 (1984).
- [11] T. Giamarchi, C. Rüegg, and O. Tchernyshyov, Bose-Einstein condensation in magnetic insulators, *Nat. Physics* **4**, 198 (2008).
- [12] V. Zapf, M. Jaime, and C. D. Batista, Bose-Einstein condensation in quantum magnets, *Rev. Mod. Phys.* **86**, 563 (2014).
- [13] V. S. Zapf, D. Zocco, B. R. Hansen, M. Jaime, N. Harrison, C. D. Batista, M. Kenzelmann, C. Niedermayer, A. Lacerda, and A. Paduan-Filho, Bose-Einstein Condensation of  $S = 1$  Nickel Spin Degrees of Freedom in  $\text{NiCl}_2\cdot 4\text{SC}(\text{NH}_2)_2$ , *Phys. Rev. Lett.* **96**, 077204 (2006).
- [14] L. Yin, J. S. Xia, V. S. Zapf, N. S. Sullivan, and A. Paduan-Filho, Direct Measurement of the Bose-Einstein Condensation Universality Class in  $\text{NiCl}_2\cdot 4\text{SC}(\text{NH}_2)_2$  at Ultralow Temperatures, *Phys. Rev. Lett.* **101**, 187205 (2008).
- [15] M. Matsumoto and M. Koga, Longitudinal spin-wave mode near quantum critical point due to uniaxial anisotropy, *J. Phys. Soc. Jap.* **76**, 073709 (2007).
- [16] M. Matsumoto, B. Normand, T. M. Rice, and M. Sigrist, Field- and pressure-induced magnetic quantum phase transitions in  $\text{TiCuCl}_3$ , *Phys. Rev. B* **69**, 054423 (2004).
- [17] Z. Zhang, K. Wierschem, I. Yap, Y. Kato, C. D. Batista, and P. Sengupta, Phase diagram and magnetic excitations of anisotropic spin-one magnets, *Phys. Rev. B* **87**, 174405 (2013).
- [18] H. D. Scammell and O. P. Sushkov, Multiple universalities in order-disorder magnetic phase transitions, *Phys. Rev. B* **95**, 094410 (2017).
- [19] D. Pekker and C. M. Varma, Amplitude/Higgs Modes in Condensed Matter Physics, *Annu. Rev. Condens. Matter Phys.* **6**, 269 (2015).
- [20] C. Rüegg, B. Normand, M. Matsumoto, A. Furrer, D. F. McMorrow, K. W. Krämer, H. U. Güdel, S. N. Gvasaliya, H. Mutka, and M. Boehm, Quantum Magnets under Pressure: Controlling Elementary Excitations in  $\text{TiCuCl}_3$ , *Phys. Rev. Lett.* **100**, 205701 (2008).
- [21] P. Merchant, B. Normand, K. W. Krämer, M. Boehm, D. F. McMorrow, and C. Rüegg, Quantum and classical criticality in a dimerized quantum antiferromagnet, *Nat. Physics* **10**, 373 (2008).
- [22] K. Goto, M. Fujisawa, H. Tanaka, Y. Uwatoko, A. Oosawa, T. Osakabe, and K. Kakurai, Pressure-Induced Magnetic Quantum Phase Transition in Gapped Spin System  $\text{KCuCl}_3$ , *J. Phys. Soc. Jpn.* **75**, 064703 (2006); K. Goto, T. Osakabe, K. Kakurai, Y. Uwatoko, A. Oosawa, J. Kawakami, and H. Tanaka, Softening of Magnetic Excitations Leading to Pressure-Induced Quantum Phase Transition in Gapped Spin System  $\text{KCuCl}_3$ , *J. Phys. Soc. Jpn.* **76**, 053704 (2007).
- [23] M. Matsumoto, T. Sakurai, Y. Hirao, H. Ohta, Y. Uwatoko, and H. Tanaka, First ESR Detection of Higgs Amplitude Mode and Analysis with Extended Spin-Wave Theory in Dimer System  $\text{KCuCl}_3$ , *Appl. Magn. Reson.* **52**, 523 (2021).
- [24] M. Thede, A. Mannig, M. Månsson, D. Hübner, R. Khasanov, E. Morenzoni, and A. Zheludev, Pressure-induced quantum critical and multicritical points in a frustrated spin liquid, *Phys. Rev. Lett.* **112**, 087204 (2014).
- [25] G. Perren, J. S. Möller, D. Hübner, A. A. Podlesnyak, and A. Zheludev, Spin dynamics in pressure-induced magnetically ordered phases in  $(\text{C}_4\text{H}_{12}\text{N}_2)\text{Cu}_2\text{Cl}_6$ , *Phys. Rev. B* **92**, 054413 (2015).
- [26] S. Bettler, G. Simutis, G. Perren, D. Blosser, S. Gvasaliya, and A. Zheludev, High-pressure Raman study of the quantum magnet  $(\text{C}_4\text{H}_{12}\text{N}_2)\text{Cu}_2\text{Cl}_6$ , *Phys. Rev. B* **96**, 174431 (2017).
- [27] T. Hong, K. P. Schmidt, K. Coester, F. F. Awwadi, M. M. Turnbull, Y. Qiu, J. A. Rodriguez-Rivera, M. Zhu, X. Ke, C. P. Aoyama, Y. Takano, H. Cao, W. Tian, J. Ma, R. Custelcean, H. D. Zhou, and M. Matsuda, Magnetic ordering induced by interladder coupling in the spin- $\frac{1}{2}$  Heisenberg two-leg ladder antiferromagnet  $\text{C}_9\text{H}_{18}\text{N}_2\text{CuBr}_4$ , *Phys. Rev. B* **89**, 174432 (2014).
- [28] T. Hong, T. Ying, Q. Huang, S. E. Dissanayake, Y. Qiu, M. M. Turnbull, A. A. Podlesnyak, Y. Wu, H. Cao, Y. Liu, I. Umehara, J. Gouchi, Y. Uwatoko, M. Matsuda, D. A. Tennant, G.-W. Chern, K. P. Schmidt, and S. Wessel, Evidence for pressure induced unconventional quantum criticality in the coupled spin ladder antiferromagnet  $\text{C}_9\text{H}_{18}\text{N}_2\text{CuBr}_4$ , *Nat. Comm.* **13**, 3073 (2022).
- [29] R. Dell'Amore, A. Schilling, and K. Krämer,  $U(1)$  symmetry breaking and violated axial symmetry in  $\text{TiCuCl}_3$  and other insulating spin systems, *Phys. Rev. B* **79**, 014438 (2009).
- [30] N. Kurita and H. Tanaka, Magnetic-field- and pressure-induced quantum phase transition in  $\text{CsFeCl}_3$  proved via magnetization measurements, *Phys. Rev. B* **94**, 104409 (2016); S. Hayashida, O. Zaharko, N. Kurita, H. Tanaka, M. Hagihara, M. Soda, S. Itoh, Y. Uwatoko, and T. Masuda, Pressure-induced quantum phase transition in the quantum antiferromagnet  $\text{CsFeCl}_3$ , *Phys. Rev. B* **97**, 140405 (2018).
- [31] S. Hayashida, M. Matsumoto, M. Hagihara, N. Kurita, H. Tanaka, S. Itoh, T. Hong, M. Soda, Y. Uwatoko, and T. Masuda, Novel excitations near quantum criticality

- in geometrically frustrated antiferromagnet  $\text{CsFeCl}_3$ , *Sci. Adv.* **5**, eaaw5639 (2019).
- [32] K. Yu. Povarov, E. Wulf, D. H  vonen, J. Ollivier, A. Paduan-Filho, and A. Zheludev, Dynamics of a bond-disordered  $S = 1$  quantum magnet near  $z = 1$  criticality, *Phys. Rev. B* **92**, 024429 (2015).
- [33] K. Yu. Povarov, A. Mannig, G. Perren, J. S. M  ller, E. Wulf, J. Ollivier, and A. Zheludev, Quantum criticality in a three-dimensional spin system at zero field and pressure, *Phys. Rev. B* **96**, 140414 (2017); A. Mannig, K. Yu. Povarov, J. Ollivier, and A. Zheludev, Spin waves near the edge of halogen substitution induced magnetic order in  $\text{Ni}(\text{Cl}_{1-x}\text{Br}_x)_2 \cdot 4\text{SC}(\text{NH}_2)_2$ , *Phys. Rev. B* **98**, 214419 (2018).
- [34] R. Yu, L. Yin, N. S. Sullivan, J. S. Xia, C. Huan, A. Paduan-Filho, N. F. Oliveira Jr, S. Haas, A. Steppke, C. F. Miclea, F. Weickert, R. Movshovich, E.-D. Mun, B. L. Scott, V. S. Zapf, and T. Roscilde, Bose glass and Mott glass of quasiparticles in a doped quantum magnet, *Nature* **489**, 379 (2012); R. Yu, C. F. Miclea, F. Weickert, R. Movshovich, A. Paduan-Filho, V. S. Zapf, and T. Roscilde, Quantum critical scaling at a Bose-glass/superfluid transition: Theory and experiment for a model quantum magnet, *Phys. Rev. B* **86**, 134421 (2012).
- [35] M. Dupont, S. Capponi, M. Horvati  , and N. Laflorencie, Competing Bose-glass physics with disorder-induced Bose-Einstein condensation in the doped  $S = 1$  antiferromagnet  $\text{Ni}(\text{Cl}_{1-x}\text{Br}_x)_2 - 4\text{SC}(\text{NH}_2)_2$  at high magnetic fields, *Phys. Rev. B* **96**, 024442 (2017).
- [36] A. Orlova, R. Blinder, E. Kermarrec, M. Dupont, N. Laflorencie, S. Capponi, H. Mayaffre, C. Berthier, A. Paduan-Filho, and M. Horvati  , Nuclear Magnetic Resonance Reveals Disordered Level-Crossing Physics in the Bose-Glass Regime of the Br-Doped  $\text{Ni}(\text{Cl}_{1-x}\text{Br}_x)_2 - 4\text{SC}(\text{NH}_2)_2$  Compound at a High Magnetic Field, *Phys. Rev. Lett.* **118**, 067203 (2017).
- [37] M. Dupont, S. Capponi, and N. Laflorencie, Disorder-Induced Revival of the Bose-Einstein Condensation in  $\text{Ni}(\text{Cl}_{1-x}\text{Br}_x)_2 - 4\text{SC}(\text{NH}_2)_2$  at High Magnetic Fields, *Phys. Rev. Lett.* **118**, 067204 (2017); A. Orlova, H. Mayaffre, S. Kr  mer, M. Dupont, S. Capponi, N. Laflorencie, A. Paduan-Filho, and M. Horvati  , Detection of a Disorder-Induced Bose-Einstein Condensate in a Quantum Spin Material at High Magnetic Fields, *Phys. Rev. Lett.* **121**, 177202 (2018).
- [38] A. B. Harris, Effect of random defects on the critical behavior of Ising models, *J. Phys. C: Solid State Phys.* **7**, 1671 (1974).
- [39] L. Facheris, D. Blosser, K. Yu. Povarov, R. Bewley, S. Gvasaliya, and A. Zheludev, Finite-temperature dynamics and the role of disorder in nearly critical  $\text{Ni}(\text{Cl}_{1-x}\text{Br}_x)_2 \cdot 4\text{SC}(\text{NH}_2)_2$ , *Phys. Rev. B* **102**, 224405 (2020).
- [40] A. Lopez-Castro and M. R. Truter, The crystal and molecular structure of dichlorotetrakis(hydroxy)nickel,  $[(\text{NH}_2)_2\text{CS}]_4\text{NiCl}_2$ , *J. Chem. Soc.*, 1309 (1963).
- [41] S. A. Zvyagin, J. Wosnitza, A. K. Kolezhuk, V. S. Zapf, M. Jaime, A. Paduan-Filho, V. N. Glazkov, S. S. Sosin, and A. I. Smirnov, Spin dynamics of  $\text{NiCl}_2 - 4\text{SC}(\text{NH}_2)_2$  in the field-induced ordered phase, *Phys. Rev. B* **77**, 092413 (2008).
- [42] V. S. Zapf, V. F. Correa, P. Sengupta, C. D. Batista, M. Tsukamoto, N. Kawashima, P. Egan, C. Pantea, A. Miglioni, J. B. Betts, M. Jaime, and A. Paduan-Filho, Direct measurement of spin correlations using magnetostriiction, *Phys. Rev. B* **77**, 020404 (2008).
- [43] A. V. Sizanov and A. V. Syromyatnikov, Bosonic representation of quantum magnets with large single-ion easy-plane anisotropy, *Phys. Rev. B* **84**, 054445 (2011).
- [44] C. Psaroudaki, S. A. Zvyagin, J. Krzystek, A. Paduan-Filho, X. Zotos, and N. Papanicolaou, Magnetic excitations in the spin-1 anisotropic antiferromagnet  $\text{NiCl}_2 - 4\text{SC}(\text{NH}_2)_2$ , *Phys. Rev. B* **85**, 014412 (2012).
- [45] A. Paduan-Filho, X. Gratens, and N. F. Oliveira, Field-induced magnetic ordering in  $\text{NiCl}_2 \cdot 4\text{SC}(\text{NH}_2)_2$ , *Phys. Rev. B* **69**, 020405 (2004).
- [46] K. Wierschem and P. Sengupta, Characterizing the Haldane phase in quasi-one-dimensional spin-1 Heisenberg antiferromagnets, *Mod. Phys. Lett. B* **28**, 1430017 (2014).
- [47] M. Orend   , S. Zvyagin, A. Orend   ov  , M. Sieling, B. L  thi, A. Feher, and M. W. Meisel, Single-ion bound states in  $S = 1$  Heisenberg antiferromagnetic chains with planar anisotropy and subcritical exchange coupling, *Phys. Rev. B* **60**, 4170 (1999).
- [48] S. Chattopadhyay, D. Jain, V. Ganesan, S. Giri, and S. Majumdar, Observation of large- $D$  magnetic phase in  $\text{Sr}_3\text{NiPtO}_6$ , *Phys. Rev. B* **82**, 094431 (2010).
- [49] A. Mannig, *Experimental studies of zero-field phase transitions in quantum magnets* (PhD thesis, ETH Z  rich, 2017).
- [50] S. A. Zvyagin, D. Graf, T. Sakurai, S. Kimura, H. Nojiri, J. Wosnitza, H. Ohta, T. Ono, and H. Tanaka, Pressure-tuning the quantum spin Hamiltonian of the triangular lattice antiferromagnet  $\text{Cs}_2\text{CuCl}_4$ , *Nat. Commun.* **10**, 1064 (2019).
- [51] Z. Shi, S. Dissanayake, P. Corboz, W. Steinhardt, D. Graf, D. M. Silevitch, H. A. Dabkowska, T. F. Rosenbaum, F. Mila, and S. Haravifard, Discovery of quantum phases in the Shastry-Sutherland compound  $\text{SrCu}_2(\text{BO}_3)_2$  under extreme conditions of field and pressure, *Nat. Commun.* **13**, 2301 (2022).
- [52] V. S. Zapf, P. Sengupta, C. D. Batista, F. Nasreen, F. Wolff-Fabris, and A. Paduan-Filho, Magnetoelectric effects in an organometallic quantum magnet, *Phys. Rev. B* **83**, 140405 (2011).
- [53] J. Jensen and A. R. Mackintosh, *Rare earth magnetism: structures and excitations*, International series of monographs on physics (Clarendon Press, U.K., 1991).
- [54] S. R. White, Density matrix formulation for quantum renormalization groups, *Phys. Rev. Lett.* **69**, 2863 (1992).
- [55] U. Schollw  ck, The density-matrix renormalization group, *Rev. Mod. Phys.* **77**, 259 (2005).
- [56] U. Schollw  ck, The density-matrix renormalization group in the age of matrix product states, *Ann. Phys.* **326**, 96 (2011).
- [57] A. F. Albuquerque, C. J. Hamer, and J. Oitmaa, Quantum phase diagram and excitations for the one-dimensional  $S = 1$  Heisenberg antiferromagnet with single-ion anisotropy, *Phys. Rev. B* **79**, 054412 (2009).
- [58] N. Papanicolaou and P. Spathis, Quantum spin-1 chains with strong planar anisotropy, *J. Phys.: Cond. Mat.* **2**, 6575 (1990).
- [59] P.-A. Lindg  rd, Correlation theory of crystal field and anisotropic exchange effects, *J. Magn. Magn. Mater.* **52**, 47 (1985); I. Zaliznyak and S. Lee, Magnetic neutron scattering, in *Modern Techniques for Characterizing Magnetic Materials*, edited by Y. Zhu (Springer US,

- Boston, MA, 2005) pp. 3–64.
- [60] T. Sakai and M. Takahashi, Effect of the Haldane gap on quasi-one-dimensional systems, *Phys. Rev. B* **42**, 4537 (1990).
  - [61] R. F. S. Hearmon, The Elastic Constants of Anisotropic Materials, *Rev. Mod. Phys.* **18**, 409 (1946).
  - [62] T. Sakurai, Y. Hirao, K. Hijii, S. Okubo, H. Ohta, Y. Uwatoko, K. Kudo, and Y. Koike, Direct Observation of the Quantum Phase Transition of  $\text{SrCu}_2(\text{BO}_3)_2$  by High-Pressure and Terahertz Electron Spin Resonance, *J. Phys. Soc. Jpn.* **87**, 033701 (2018).
  - [63] T. A. Soldatov, A. I. Smirnov, K. Yu. Povarov, A. Paduan-Filho, and A. Zheludev, Microwave dynamics of the stoichiometric and bond-disordered anisotropic  $S = 1$  chain antiferromagnet  $\text{NiCl}_2-4\text{SC}(\text{NH}_2)_2$ , *Phys. Rev. B* **101**, 104410 (2020).
  - [64] R. A. Muniz, Y. Kato, and C. D. Batista, Generalized spin-wave theory: Application to the bilinear-biquadratic model, *Progr. Theor. Exp. Phys* **2014**, 1 (2014).
  - [65] S. A. Sherbakov and O. I. Utesov, Magnon spectrum and electron spin resonance in antiferromagnet with large single-ion easy plane anisotropy, *J. Magn. Magn. Mater.* **518**, 167390 (2021).
  - [66] E. Wulf, D. H  vonen, J.-W. Kim, A. Paduan-Filho, E. Ressouche, S. Gvasaliya, V. Zapf, and A. Zheludev, Criticality in a disordered quantum antiferromagnet studied by neutron diffraction, *Phys. Rev. B* **88**, 174418 (2013).
  - [67] E. Wulf, D. H  vonen, R. Sch  nemann, H. K  hne, T. Herrmannsd  rfer, I. Glavatsky, S. Gerischer, K. Kiefer, S. Gvasaliya, and A. Zheludev, Critical exponents and intrinsic broadening of the field-induced transition in  $\text{NiCl}_2-4\text{SC}(\text{NH}_2)_2$ , *Phys. Rev. B* **91**, 014406 (2015).
  - [68] N. Tsyrlin, C. D. Batista, V. S. Zapf, M. Jaime, B. R. Hansen, C. Niedermayer, K. C. Rule, K. Habicht, K. Prokes, K. Kiefer, E. Ressouche, A. Paduan-Filho, and M. Kenzelmann, Neutron study of the magnetism in  $\text{NiCl}_2-4\text{SC}(\text{NH}_2)_2$ , *J. Phys.: Condens. Matter* **25**, 216008 (2013).
  - [69] H. D. Scammell and O. P. Sushkov, Asymptotic freedom in quantum magnets, *Phys. Rev. B* **92**, 220401 (2015); Nonequilibrium quantum mechanics: A “hot quantum soup” of paramagnons, *Phys. Rev. B* **95**, 024420 (2017).
  - [70] T. Hong, Y. Qiu, M. Matsumoto, D. A. Tennant, K. Coester, K. P. Schmidt, F. F. Awwadi, M. M. Turnbull, H. Agrawal, and A. L. Chernyshev, Field induced spontaneous quasiparticle decay and renormalization of quasiparticle dispersion in a quantum antiferromagnet, *Nat. Comm.* **8**, 15148 (2017).
  - [71] H. D. Scammell, Y. Kharkov, Y. Q. Qin, Z. Y. Meng, B. Normand, and O. P. Sushkov, Unifying static and dynamic properties in three-dimensional quantum antiferromagnets, *Phys. Rev. B* **96**, 174414 (2017).
  - [72] Y. Q. Qin, B. Normand, A. W. Sandvik, and Z. Y. Meng, Amplitude Mode in Three-Dimensional Dimerized Antiferromagnets, *Phys. Rev. Lett.* **118**, 147207 (2017).
  - [73] H. Scammell, *Interplay of Quantum and Statistical Fluctuations in Critical Quantum Matter* (PhD thesis, University of New South Wales, 2017).
  - [74] D. H  vonen, S. Zhao, M. M  nsson, T. Yankova, E. Ressouche, C. Niedermayer, M. Laver, S. N. Gvasaliya, and A. Zheludev, Field-induced criticality in a gapped quantum magnet with bond disorder, *Phys. Rev. B* **85**, 100410 (2012); D. H  vonen, S. Zhao, G. Ehlers, M. M  nsson, S. N. Gvasaliya, and A. Zheludev, Excitations in a quantum spin liquid with random bonds, *Phys. Rev. B* **86**, 214408 (2012); D. H  vonen, G. Ballon, and A. Zheludev, Field-concentration phase diagram of a quantum spin liquid with bond defects, *Phys. Rev. B* **88**, 094402 (2013).
  - [75] V. N. Glazkov, G. Skoblin, D. H  vonen, T. S. Yankova, and A. Zheludev, Formation of gapless triplets in the bond-doped spin-gap antiferromagnet  $(\text{C}_4\text{H}_{12}\text{N}_2)(\text{Cu}_2\text{Cl}_6)$ , *J. Phys.: Condens. Matter* **26**, 486002 (2014); V. N. Glazkov, Y. V. Krasnikova, D. H  vonen, and A. Zheludev, Formation of the  $S = 1$  paramagnetic centers in the bond-diluted spin-gap magnet, *J. Phys.: Condens. Matter* **28**, 206003 (2016).
  - [76] A. Mannig, J. S. M  ller, M. Thede, D. H  vonen, T. Lancaster, F. Xiao, R. C. Williams, Z. Guguchia, R. Khasanov, E. Morenzoni, and A. Zheludev, Effect of disorder on a pressure-induced  $z = 1$  magnetic quantum phase transition, *Phys. Rev. B* **94**, 144418 (2016).
  - [77] J. S. Kinyon, N. S. Dalal, R. J. Clark, H. Zhou, and K. Y. Choi, Closing the spin gap of  $(\text{NH}_4)_x\text{K}_{1-x}\text{CuCl}_3$  through chemical substitution, *Phys. Rev. Mater.* **5**, 054413 (2021).
  - [78] S. Hayashida, L. Stoppel, Z. Yan, S. Gvasaliya, A. Podlesnyak, and A. Zheludev, Chemical composition induced quantum phase transition in  $\text{Cs}_{1-x}\text{Rb}_x\text{FeCl}_3$ , *Phys. Rev. B* **99**, 224420 (2019).
  - [79] A. Paduan-Filho, R. D. Chirico, K. O. Joun, and R. L. Carlin, Field-induced magnetic ordering in uniaxial nickel systems: A second example, *J. Chem. Phys.* **74**, 4103 (1981).
  - [80] T. Yankova, D. H  vonen, S. M  hlbauer, D. Schmidiger, E. Wulf, S. Zhao, A. Zheludev, T. Hong, V. O. Garlea, R. Custelcean, and G. Ehlers, Crystals for neutron scattering studies of quantum magnetism, *Philos. Mag.* **92**, 2629 (2012).
  - [81] J. Rodr  guez-Carvajal, Recent advances in magnetic structure determination by neutron powder diffraction, *Physica B* **192**, 55 (1993).
  - [82] R. B. Clover and W. P. Wolf, Magnetic Susceptibility Measurements with a Tunnel Diode Oscillator, *Rev. Sci. Instr.* **41**, 617 (1970).
  - [83] G. J. Piermarini, S. Block, J. D. Barnett, and R. A. Forman, Calibration of the pressure dependence of the R1 ruby fluorescence line to 195 kbar, *J. Appl. Phys.* **46**, 2774 (1975).
  - [84] T. Sakurai, H. Ohta, S. Hara, and Y. Saito, High-Pressure THz ESR, *Appl. Magn. Reson.* **52**, 267 (2021).
  - [85] T. Sakurai, S. Kimura, M. Kimata, H. Nojiri, S. Awaji, S. Okubo, H. Ohta, Y. Uwatoko, K. Kudo, and Y. Koike, Development and application of 2.5 GPa-25 T high-pressure high-field electron spin resonance system using a cryogen-free superconducting magnet, *J. Magn. Reson.* **296**, 1 (2018).
  - [86] T. F. Smith and C. W. Chu, Will Pressure Destroy Superconductivity?, *Phys. Rev.* **159**, 353 (1967).
  - [87] T. Sakurai, K. Fujimoto, R. Matsui, K. Kawasaki, S. Okubo, H. Ohta, K. Matsubayashi, Y. Uwatoko, and H. Tanaka, Development of multi-frequency ESR system for high-pressure measurements up to 2.5 GPa, *J. Magn. Reson.* **259**, 108 (2015).
  - [88] J. Bezanson, A. Edelman, S. Karpinski, and V. Shah, Julia: A Fresh Approach to Numerical Computing, *SIAM*

- Rev. **59**, 65 (2017).
- [89] M. Fishman, S. R. White, and E. M. Stoudenmire, The ITensor Software Library for Tensor Network Calculations, *SciPost Phys. Codebases* , 4 (2022).

# Supplemental Material for the manuscript

## Pressure-driven gapped-to-gapless phase transition in a quantum antiferromagnet with large planar anisotropy

K. Yu. Povarov,<sup>1,\*</sup> D. E. Graf,<sup>2</sup> V. O. Garlea,<sup>3</sup> T. Sakurai,<sup>4</sup> S. Kimura,<sup>5</sup> H. Nojiri,<sup>5</sup>  
A. Paduan-Filho,<sup>6</sup> A. Zheludev,<sup>7</sup> J. Wosnitzer,<sup>1,8</sup> H. Ohta,<sup>9,10</sup> and S. A. Zvyagin<sup>1,†</sup>

<sup>1</sup>*Dresden High Magnetic Field Laboratory (HLD-EMFL) and Würzburg-Dresden Cluster of Excellence *ct.qmat*,  
Helmholtz-Zentrum Dresden-Rossendorf, 01328 Dresden, Germany*

<sup>2</sup>*National High Magnetic Field Laboratory, Tallahassee, Florida 32310, USA*

<sup>3</sup>*Neutron Scattering Division, Oak Ridge National Laboratory, Oak Ridge, TN 37831, USA*

<sup>4</sup>*Research Facility Center for Science and Technology, Kobe University, Kobe, 657-8501, Japan*

<sup>5</sup>*Institute for Materials Research, Tohoku University, Sendai 980-8578, Japan*

<sup>6</sup>*Instituto de Física, Universidade de São Paulo, 05315-970 São Paulo, Brazil*

<sup>7</sup>*Laboratory for Solid State Physics, ETH Zürich, Switzerland*

<sup>8</sup>*Institut für Festkörper- und Materialphysik, Technische Universität Dresden, 01062 Dresden, Germany*

<sup>9</sup>*Molecular Photoscience Research Center, Kobe University, Kobe 657-8501, Japan*

<sup>10</sup>*Graduate School of Science, Kobe University, Kobe 657-8501, Japan*

(Dated: April 21, 2023)

This Supplemental Material contains details of neutron diffraction experiments under pressure, estimates of lattice compressibility, the numerical/analytical *ansatz* used to describe the first critical field, and various fit procedures.

### CONTENTS

I. Neutron diffraction experiments	1
II. Elastic constants	1
A. Hydrostatic pressure vs uniaxial strain	3
B. Experimental results	3
III. Critical-field fits	3
IV. Gap-magnitude estimation	4
A. DMRG results	4
B. Critical coupling from RPA	4
C. The gap in 3D	5
V. Fitting the experimental phase boundaries	5
References	6

### I. NEUTRON DIFFRACTION EXPERIMENTS

The neutron diffraction experiments with powder samples were performed at instrument HB2a, at the High Flux Isotope Reactor, Oak Ridge National Laboratory (Tennessee, USA). Up to few grams of deuterated DTN powder material were used. The Ge[113] or Ge[115] vertically focussing wafer-stack monochromator was used to produce a neutron beam with 2.41 Å or 1.54 Å wavelength. A <sup>4</sup>He Orange cryostat with aluminum He gas

pressure cell (up to 6 kbar), or a CuBe clamp cell (up to 20 kbar) was used as the sample environment.

The pressure in the gas cell was directly measured *in situ* with the manometer. For the clamp cell a rock salt calibration curve was used for the achieved pressure estimate, resulting in the  $\sim 1$  kbar errorbar.

Examples of the measured diffraction data (scattered neutron beam intensity vs momentum transfer) can be found in Fig. S1. After the initial data reduction, the FULLPROF package [1] was used for the intensity-profile analysis and structure determination. Examples of the fits are shown in Fig. S2. At small pressures the peak pattern remains qualitatively the same for all the temperatures used, only the lattice constants are shrinking gradually. The situation changes at around  $P_{\text{irr}} \simeq 6$  kbar. Extra Bragg peaks appear, signalling the doubling of the structural unit cell. These peaks are not vanishing upon releasing the pressure [Fig. S1(b)], evidencing the irreversible character of the phase transition. This distorted phase above  $P_{\text{irr}}$  has been characterized as well. While the distances in the Ni<sup>2+</sup> tetragonal unit stay nearly constant, noticeable changes occur for the thiourea ligands. They start rotating and are responsible for forming a “superstructure” atop the basic DTN lattice. A more detailed analysis is given in Ref. [2].

### II. ELASTIC CONSTANTS

Under a hydrostatic-pressure conditions the relation between the length reduction and a Young’s modulus at the given direction is not straightforward. Let us derive the corresponding equations prior to discussing the experimentally measured lattice-parameters change under pressure.

\* k.povarov@hzdr.de; Previous address: Laboratory for Solid State Physics, ETH Zürich, Switzerland

† s.zvyagin@hzdr.de

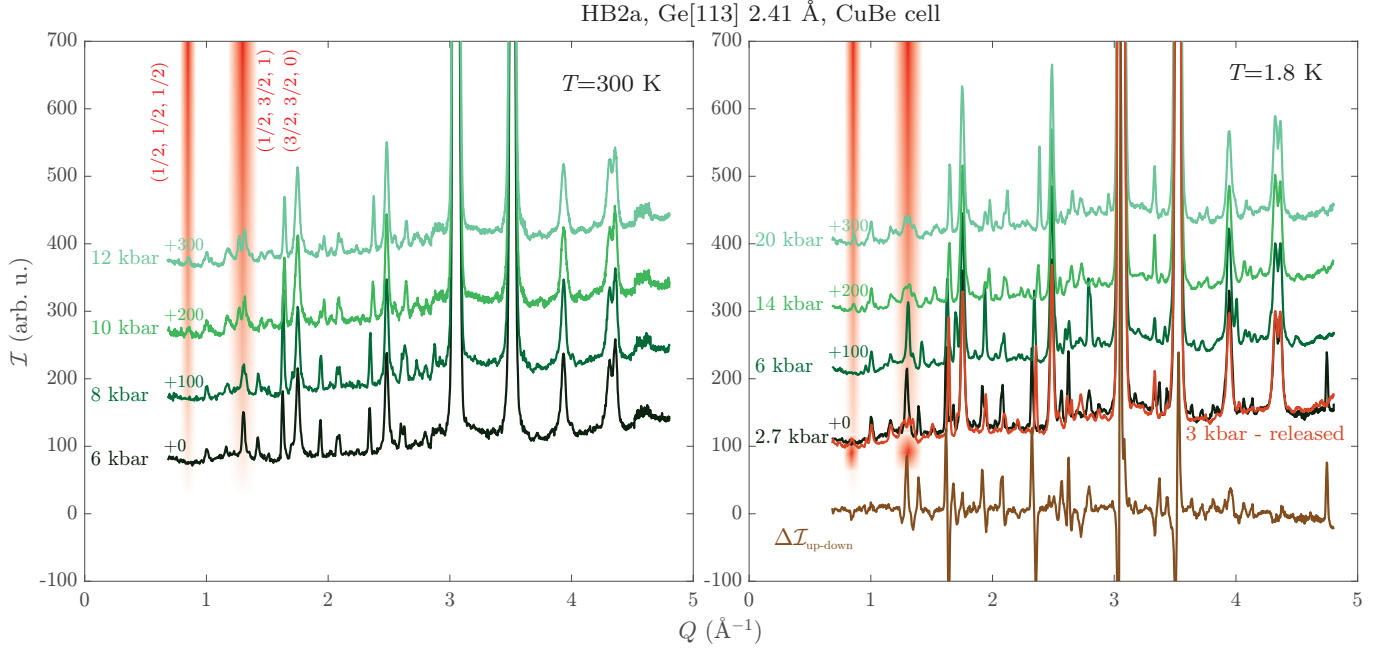


FIG. S1. Measured neutron-diffraction intensity vs momentum transfer at different pressures, (a) at 300 K, and (b) at 1.8 K. Clamp cell was used in either case. The pressures are indicated on the plots, as well as the intensity offsets used for clarity. Red color is used to highlight the superstructure peaks emerging at high pressure. In (b), the 3 kbar curve obtained after the pressure release, is overlaid with the 2.7 kbar curve obtained at the initial loading cycle. The intensity difference between these two measurements is plotted below. This data was originally presented in Ref. [2].

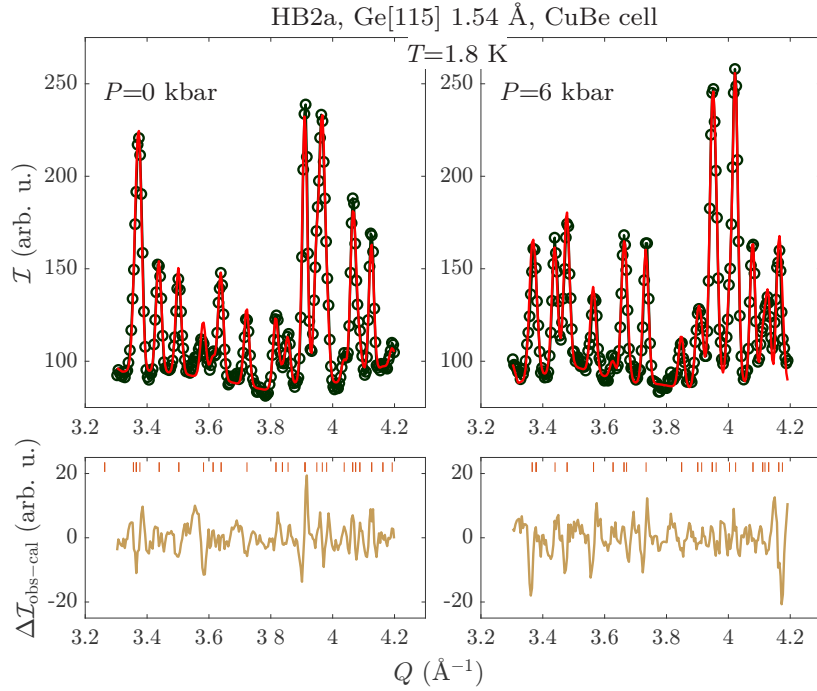


FIG. S2. Examples of fits (red lines) to the powder diffraction data (open circles) of DTN at ambient pressure and at 6 kbar. Bottom panels show the residues and the expected Bragg peak positions. This data was originally presented in Ref. [2]

### A. Hydrostatic pressure vs uniaxial strain

Let us examine the elasticity-theory equations for the tetragonal crystal in two different scenarios: hydrostatic pressure and uniaxial strain (in  $x$  or  $z$  direction). The equations that define the relation between the stress  $\sigma$  and the strain  $\varepsilon$  can be reduced to a 3-by-3 matrix equation if we neglect the shear components, which is appropriate in either case:

$$\begin{pmatrix} \sigma_x \\ \sigma_y \\ \sigma_z \end{pmatrix} = \mathbb{C} \begin{pmatrix} \varepsilon_x \\ \varepsilon_y \\ \varepsilon_z \end{pmatrix}. \quad (\text{S.1})$$

Here, the elasticity matrix  $\mathbb{C}$  is composed of several symmetry-allowed elastic moduli:

$$\mathbb{C} = \begin{pmatrix} c_{xx} & c_{xy} & c_{xz} \\ c_{xy} & c_{xx} & c_{xz} \\ c_{xz} & c_{xz} & c_{zz} \end{pmatrix}. \quad (\text{S.2})$$

The inverse problem  $\vec{\varepsilon} = \mathbb{S}\vec{\sigma}$  is formulated with the help of the compliance matrix  $\mathbb{S} = \mathbb{C}^{-1}$ , that has the same symmetry. The compliance-matrix components are [3]:

$$\begin{aligned} s_{xx} &= \frac{c_{xx}c_{zz} - c_{xz}^2}{c_0(c_{xx} - c_{xy})}, \\ s_{zz} &= \frac{c_{xx} + c_{xy}}{c_0}, \\ s_{xy} &= \frac{c_{xz}^2 - c_{xy}c_{zz}}{c_0(c_{xx} - c_{xy})}, \\ s_{xz} &= -\frac{c_{xz}}{c_0}, \end{aligned} \quad (\text{S.3})$$

$$\text{with } c_0 = c_{zz}(c_{xx} + c_{xy}) - 2c_{xz}^2.$$

For a uniaxial stress applied in  $x$  direction,  $\vec{\sigma} = (P, 0, 0)$ , the strain along that direction would be:

$$\varepsilon_x = s_{xx}P.$$

For the  $z$  direction, with  $\vec{\sigma} = (0, 0, P)$  correspondingly

$$\varepsilon_z = s_{zz}P.$$

This gives us the conventional Young's moduli

$$E_{xx} = s_{xx}^{-1} = c_{xx} - c_{xy} + \frac{(c_{zz}c_{xy} + c_{xz}^2)(c_{xx} - c_{xy})}{c_{xx}c_{zz} - c_{xz}^2}, \quad (\text{S.4})$$

and

$$E_{zz} = s_{zz}^{-1} = c_{zz} - 2\frac{c_{xz}^2}{c_{xx} + c_{xy}}. \quad (\text{S.5})$$

Under the hydrostatic pressure the compression is different. The stress is  $\vec{\sigma} = (P, P, P)$ , and the strain is  $\vec{\varepsilon} = (\varepsilon_x, \varepsilon_x, \varepsilon_z)$ . For the strain components, we find:

$$\begin{aligned} \varepsilon_x &= (s_{xx} + s_{xy} + s_{xz})P = \frac{c_{zz} - c_{xz}}{c_{zz}(c_{xx} + c_{xy}) - 2c_{xz}^2}P, \\ \varepsilon_z &= (2s_{xz} + s_{zz})P = \frac{c_{xx} + c_{xy} - 2c_{xz}}{c_{zz}(c_{xx} + c_{xy}) - 2c_{xz}^2}P. \end{aligned} \quad (\text{S.6})$$

Hence, under the hydrostatic conditions our pressure-to-strain ratios are:

$$\left[ \frac{\Delta P}{\Delta a/a} \right] = \frac{c_{zz}(c_{xx} + c_{xy}) - 2c_{xz}^2}{c_{zz} - c_{xz}}, \quad (\text{S.7})$$

$$\left[ \frac{\Delta P}{\Delta c/c} \right] = \frac{c_{zz}(c_{xx} + c_{xy}) - 2c_{xz}^2}{c_{xx} + c_{xy} - 2c_{xz}}. \quad (\text{S.8})$$

Note, that from Eqs. (S.5) and (S.8) follows  $\left[ \frac{\Delta P}{\Delta c/c} \right] = E_{zz} \frac{c_{xx} + c_{xy}}{c_{xx} + c_{xy} - 2c_{xz}}$ . We obtain a significant boost in the compression compared to the uniaxial case thanks to off-diagonal components of the elasticity matrix.

### B. Experimental results

As demonstrated above, the hydrostatic compressibility modulus for the  $c$  direction is:

$$\left[ \frac{\Delta P}{\Delta c/c} \right] = E_{zz} \frac{c_{xx} + c_{xy}}{c_{xx} + c_{xy} - 2c_{xz}}. \quad (\text{S.9})$$

Here,  $E_{zz}$  is the true Young's modulus for longitudinal stress, and  $c_{\alpha\beta}$  are the various elastic moduli. According to Zapf *et al.* [4], these moduli are  $c_{xx} = 26.1$  GPa,  $c_{xy} = 15.3$  GPa, and  $c_{xz} = 12.4$  GPa, yielding the factor 4.76 in Eq. (S.9). We find  $\left[ \frac{\Delta P}{\Delta c/c} \right] = 23.1 \pm 1.7$  GPa, hence  $E_{zz} = 4.9 \pm 0.4$  GPa. This is reasonably close to the value  $7.5 \pm 0.7$  GPa that Zapf *et al.* reported [4]. Possible systematic errors in the determination of the elastic moduli  $c_{\alpha\beta}$  would affect either estimate.

In the  $a$  direction, DTN appears to be much harder, and the reduction of this lattice constant is an order of magnitude weaker:  $\partial a / \partial P = (-4.1 \pm 1.5) \cdot 10^{-3}$  Å/kbar.

### III. CRITICAL-FIELD FITS

Here, we describe the fits of the tunnel diode oscillator (TDO) frequency shift data, shown in Fig. 3 of the main text. For the low-field step-like anomaly, we use the following (purely empirical) fit function:

$$\frac{\Delta\nu}{\langle\nu\rangle} = \left[ \frac{\Delta\nu}{\langle\nu\rangle} \right]_1 + \eta_1 H + \frac{A_1}{2} \left\{ 1 + \operatorname{erf} \left( \frac{H - H_{c1}}{\delta H_1 \sqrt{2}} \right) \right\}. \quad (\text{S.10})$$

$$\frac{\Delta\nu}{\langle\nu\rangle} = \left[ \frac{\Delta\nu}{\langle\nu\rangle} \right]_2 + \eta_2 H + \begin{cases} \frac{A_2}{\delta H_2 \sqrt{2\pi}} \exp \left[ -\frac{1}{2} \left( \frac{H - H_{c2}}{\delta H_2} \right)^2 \right], & H \geq H_{c2} \\ B + \frac{A'}{(H_\infty - H)^\alpha}, & H < H_{c2} \end{cases}. \quad (\text{S.11})$$

Here, the high-field sharp half of the peak is described by a Gaussian distribution of weight  $A_2$  and width  $\delta H_2$ , centered right at  $H_{c2}$ . Below this critical field, the broad part is better captured by the generalized hyperbola, centered at some effective field  $H_\infty > H_{c2}$ , with the amplitude  $A'$  and the characteristic exponent  $\alpha$ . The offset  $B = \frac{A_2}{\delta H_2 \sqrt{2\pi}} - \frac{A'}{(H_\infty - H_{c2})^\alpha}$  ensures the curve is continuous at  $H_{c2}$ . The linear background, characterized by  $\left[ \frac{\Delta\nu}{\langle\nu\rangle} \right]_2$  and  $\eta_2$ , is the same for both pieces of the curve. This is the background that is subtracted from the full range of the data in order to yield the detrended version of the plots actually shown in Fig. 3. This is a meaningful treatment of at least the high-field part of the background, since any sample-related susceptibility picked up by the TDO circuit vanishes there at low temperatures.

#### IV. GAP-MAGNITUDE ESTIMATION

##### A. DMRG results

As described in the main text, we have simulated a  $N = 249$  sites  $S = 1$  chain, using density matrix renormalization group (DMRG) technique implementation in Julia version of ITensors package (30 sweeps, energy convergence better than  $10^{-6}$ ). In particular, it allows a straightforward gap-size estimation. At a first step, the ground state vector in the Hilbert space of the model is found, which is a conventional DMRG routine. In the next step, this ground state is excluded from the Hilbert space, and the DMRG procedure is repeated once again. Naturally, the lowest energy state yielded is then the first excited state. The energy difference between the two respective states is directly the energy gap  $\Delta_0$ . The results in the full range of parameters are shown in Fig. S3. They provide a good interpolation between the two known limits: the large- $D$  generalized spin-wave theory (GSWT) formula  $\sqrt{D^2 - 4DJ_c/J_c}$  [5–7] and spin-gap critical behavior  $0.52(D/J_c - 0.971)^{1.478}$  [8].

Here, the first two terms describe the linear background, and the step-like part is described by the Gaussian error function centered at the first critical field  $H_{c1}$ . The parameter  $\delta H_1$  controls the transition width.

The second critical field is more involved, as one has to deal with an asymmetric peak there. We find that the following construction allows us to fit the data quite well:

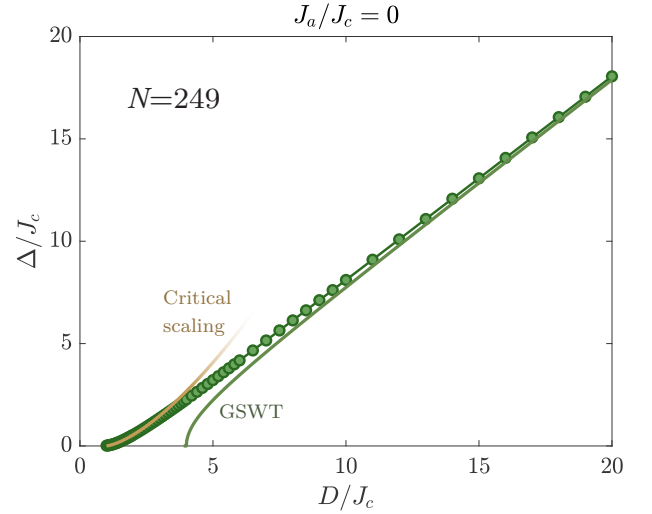


FIG. S3. The gap in the quantum-disordered (QD) phase of the 1D model, as calculated by DMRG. Points are the results of numeric calculations; the solid lines are GSWT result valid for large  $D$ , and the critical gap scaling near  $D/J_c \simeq 1$  found by Albuquerque *et al.* [8]. Our DMRG data nicely interpolates between these two regimes.

##### B. Critical coupling from RPA

Here, we give a detailed description of the random phase approximation (RPA)-based *ansatz* we used to calculate the gap (and, hence,  $H_{c1}$ ) as a function of pressure. First, we need to start with RPA (or a mean field, if one prefers such notation) expression for the transverse staggered susceptibility [9]:

$$\chi_{xx}^{\text{RPA}}(\mathbf{Q}) = \frac{\chi_{xx}^{\text{1D}}(\pi/c)}{1 - 4J_a \chi_{xx}^{\text{1D}}(\pi/c)}. \quad (\text{S.12})$$

Here, the 3D antiferromagnetic propagation vector is  $\mathbf{Q} = (\pi/a, \pi/a, \pi/c)$ , and  $\chi_{xx}^{\text{1D}}(\pi/c)$  is the transverse staggered susceptibility of a single chain. Eq. S.12 is the

susceptibility that is meant to diverge once we enter the domain of XY AF order.

In order to evaluate this quantity, we make use of a certain dynamic structure-factor approximations for large  $D$ , and the Kramers–Kronig relations. We start with making a useful RPA-type approximation for the transverse dynamic structure factor in a large- $D$  chain of  $N$  sites:

$$\mathcal{S}^{xx}(\pi/c, \omega) = N \frac{AD}{\Delta_0} \delta(\Delta_0 - \omega). \quad (\text{S.13})$$

The dispersion relation has a minimum at wavevector  $\pi/c$ , and this is exactly the gap  $\Delta_0$ . The amplitude prefactor  $\mathcal{A}$  is, generally, a complex quantity that depends on  $D$  and  $J_c$ , as well as on various on-site and inter-site ground-state correlators  $\langle (\hat{S}^x)^2 \rangle$  and  $\langle \hat{S}_n^\alpha \hat{S}_{n+1}^\alpha \rangle$ , with  $\alpha = x, z$  [10, 11]. However, in first approximation this is merely  $\mathcal{A} = 1 + \mathcal{O}(J_c/D)$ . Treating  $\mathcal{A}$  as a constant somewhat larger than 1 is the approximation we make in our *ansatz* beyond conventional RPA.

Then, at  $T = 0$  the fluctuation-dissipation theorem dictates that the dissipative part of the transverse staggered susceptibility is:

$$\chi''_{xx}(\pi/c, \omega) = \frac{\pi}{N} \mathcal{S}^{xx}(\pi/c, \omega) = \frac{\pi \mathcal{A} D}{\Delta_0} \delta(\Delta_0 - \omega).$$

With this, we can take advantage of the Kramers–Kronig relation in order to evaluate the desired static susceptibility. The latter is equivalent to the reactive part at  $\omega = 0$ :

$$\chi'_{xx}(\pi/c, 0) = \frac{1}{\pi} \int_{-\infty}^{+\infty} \frac{\pi \mathcal{A} D}{\Delta_0} \frac{\delta(\Delta_0 - \Omega)}{\Omega} d\Omega \quad (\text{S.14})$$

We, thus, arrive at the estimate for the 1D critical susceptibility:

$$\chi'_{xx}(\pi/c) = \frac{AD}{\Delta_0^2}, \quad (\text{S.15})$$

which, combined with the RPA expression (S.12) gives us the ordering criterion:

$$4J_a \frac{AD}{\Delta_0^2} = 1. \quad (\text{S.16})$$

This is exactly the criterion (4) from the main text.

### C. The gap in 3D

The next step is to estimate the influence of the  $J_a$  bonds on the spin gap  $\Delta_0$ . For this, we write an RPA analogue of Eq. (S.15):

$$\chi'^{\text{RPA}}_{xx}(\pi/c) = \frac{AD}{\Delta_{3D}^2}, \quad (\text{S.17})$$

Leaving the factor  $\mathcal{A}$  unchanged (which is another approximation), and making use of the general formula (S.13), we arrive at:

$$\Delta_{3D}^2 = \Delta_0^2 - 4ADJ_a. \quad (\text{S.18})$$

We can rewrite this in terms of a critical coupling  $J_a^{\text{crit}}$  defined for given  $D$  and  $J_c$  (S.16):

$$\Delta_{3D}^2 = \Delta_0^2 - \Delta_0^2 \frac{J_a}{J_a^{\text{crit}}}. \quad (\text{S.19})$$

This is the Eq. (5) from the main text.

## V. FITTING THE EXPERIMENTAL PHASE BOUNDARIES

A given set of Hamiltonian (1) parameters is represented by a single point in the Sakai–Takahashi phase diagram plane (Fig. 5(b) of the main text) [12]. With  $D$  and  $J_c$  changing linearly with the pressure, and  $J_a$  being constant, this point would move along the nearly straight line. The slope of the line is given by the ratio between  $\partial D/\partial P$  and  $\partial J_c/\partial P$ . Since the pressure dependence of  $H_{c2}$  locks the linear relationship between these quantities, this is a single-parameter problem. Suggesting a particular value of  $P_c$  unambiguously fixes the magnitudes of  $\partial D/\partial P$  and  $\partial J_c/\partial P$ , so that the point representing the Hamiltonian crosses the critical line at this pressure. Thus obtained pairs of parameters for different choices of  $P_c$  are shown in Fig. S4(b) in the magnetostriction notation. We can conclude that the value of  $P_c$  remains *the only parameter* in the description of the experimental data. Naturally, the criterion for better  $P_c$  quantification is the quality of agreement to the experimentally observed  $H_{c1}$  values. We are considering the mean-square deviation

$$\chi^2 = \mu_0 \sqrt{\sum (H_{c1}^{\text{obs}} - H_{c1}^{\text{calc}})^2}, \quad (\text{S.20})$$

with the calculated values obtained from our *ansatz*. This quantity is shown in Fig S4(a). The optimal overlap is found in the range  $P_c = 4.3 \pm 0.3$  kbar, which gives us  $k_B^{-1} \partial D/\partial z = -4.1 \pm 0.7$  and  $k_B^{-1} \partial J_c/\partial z = -6.5 \pm 0.3$  K/Å.

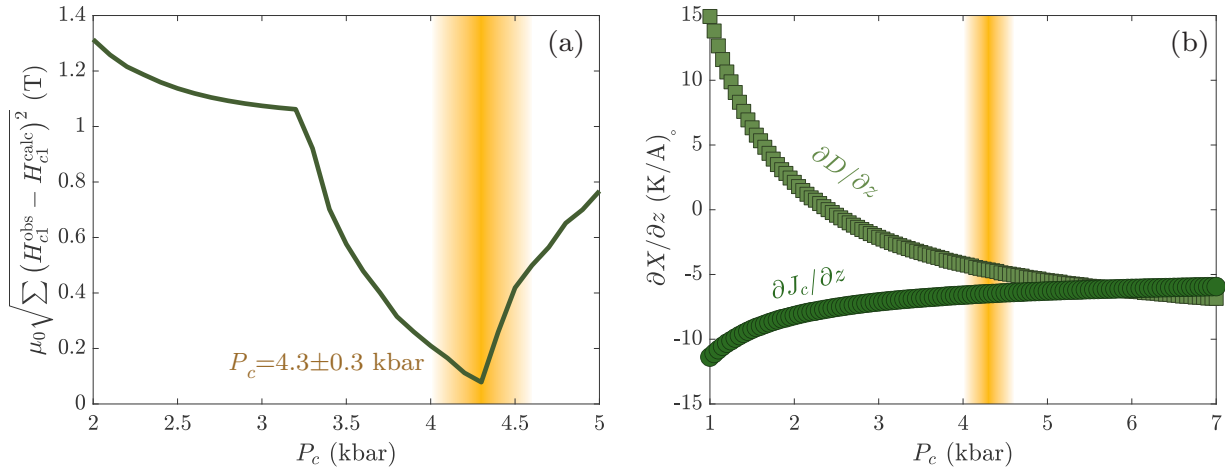


FIG. S4. (a) Mean-square deviation between the RPA *ansatz* fit and the actually observed values of  $H_{c1}$  as a function of critical pressure we assign to our model. The agreement is optimized around  $P_c \simeq 4.3$  kbar; the error bar represents the approximate threshold at which the  $\chi^2$  value (see Eq. (S.20)) doubles compared to the minimal value. (b) The magnetostriction coefficients as a function of model critical pressure. The optimal region is highlighted.

- 
- [1] J. Rodríguez-Carvajal, Recent advances in magnetic structure determination by neutron powder diffraction, *Physica B* **192**, 55 (1993).
  - [2] A. Mannig, *Experimental studies of zero-field phase transitions in quantum magnets* (PhD thesis, ETH Zürich, 2017).
  - [3] R. F. S. Hearmon, The Elastic Constants of Anisotropic Materials, *Rev. Mod. Phys.* **18**, 409 (1946).
  - [4] V. S. Zapf, V. F. Correa, P. Sengupta, C. D. Batista, M. Tsukamoto, N. Kawashima, P. Egan, C. Pantea, A. Migliori, J. B. Betts, M. Jaime, and A. Paduan-Filho, Direct measurement of spin correlations using magnetostriction, *Phys. Rev. B* **77**, 020404 (2008).
  - [5] N. Papanicolaou and P. Spathis, Quantum spin-1 chains with strong planar anisotropy, *J. Phys.: Cond. Mat.* **2**, 6575 (1990).
  - [6] M. Matsumoto and M. Koga, Longitudinal spin-wave mode near quantum critical point due to uniaxial anisotropy, *J. Phys. Soc. Jap.* **76**, 073709 (2007).
  - [7] Z. Zhang, K. Wierschem, I. Yap, Y. Kato, C. D. Batista, and P. Sengupta, Phase diagram and magnetic excitations of anisotropic spin-one magnets, *Phys. Rev. B* **87**, 174405 (2013).
  - [8] A. F. Albuquerque, C. J. Hamer, and J. Oitmaa, Quantum phase diagram and excitations for the one-dimensional  $S = 1$  Heisenberg antiferromagnet with single-ion anisotropy, *Phys. Rev. B* **79**, 054412 (2009).
  - [9] J. Jensen and A. R. Mackintosh, *Rare earth magnetism: structures and excitations*, International series of monographs on physics (Clarendon Press, U.K., 1991).
  - [10] P.-A. Lindgård, Correlation theory of crystal field and anisotropic exchange effects, *J. Magn. Magn. Mater.* **52**, 47 (1985).
  - [11] I. Zaliznyak and S. Lee, Magnetic neutron scattering, in *Modern Techniques for Characterizing Magnetic Materials*, edited by Y. Zhu (Springer US, Boston, MA, 2005) pp. 3–64.
  - [12] T. Sakai and M. Takahashi, Effect of the Haldane gap on quasi-one-dimensional systems, *Phys. Rev. B* **42**, 4537 (1990).